

Ultrafast antiferromagnetic domain switching in NiO induced by spin transfer torques

Théophile Chirac,^{1,*} Jean-Yves Chauleau,^{1,†} Pascal Thibaudeau,^{2,‡} and Michel Viret^{1,§}

¹CEA Saclay, DSM/IRAMIS/SPEC, URA CNRS 2464, 91191 Gif-sur-Yvette, France

²CEA-DAM-Le Ripault, BP 16, F-37260, Monts, France

(Dated: April 23, 2022)

NiO is a prototypical antiferromagnet with a characteristic resonance frequency in the THz range. Using the spin transfer torque mechanism, we describe antiferromagnetic switching at this frequency, thus opening the possibility to speed up current logic of electronic devices by several orders of magnitude. We use atomistic spin dynamics simulations taking into account the crystallographic structure of NiO and in particular using a magnetic anisotropy respecting its symmetry. Sub-picosecond S-domain switching between the six allowed stable spin directions is found for reasonably achievable spin currents. We thus describe a simple procedure for picosecond writing of a six state memory and comment on the consequences for a possible NiO based antiferromagnetic oscillator.

I. INTRODUCTION

Nature provides us with a variety of magnetic textures and antiferromagnetism occurs commonly among transition metal compounds, especially oxides. It consists in a local combination of magnetic moments of several ions in crystalline sublattices to produce a vanishing total magnetization. As a consequence, such antiferromagnetic (AF) materials display several interesting characteristics including insensitivity to external magnetic perturbations and, thanks to the intensity of the exchange interaction, picosecond dynamics, which make them promising for a new generation of ultrafast spintronic devices¹.

The past ten years have seen a surge of interest, mainly at a fundamental level, to bring proofs of concept for their use as memory devices. Early theories targeted antiferromagnetic metals²⁻⁴ and inspired their validation as memory devices^{5,6}. However, insulators may be better candidates as they exhibit lower magnetization damping, they are spin conductors controllable by spin currents⁷⁻⁹. Many materials are candidates for building a memory device but so far, NiO has attracted the most attention and is considered an archetype for applications at room-temperature. Nevertheless, it is surprising that none of the published works aiming at using this material in spintronics, considers its real natural crystallographic form. Indeed, NiO is quite systematically approximated as a uniaxial antiferromagnet or at best, an single easy axis easy plane compound¹⁰. While it is known that NiO indeed possesses a hard magnetic axis, its subsequent planar anisotropy has tri-axial symmetry¹¹. This complicates a straightforward description of the magnetic properties of this compound, but it also potentially offers a richer switching behavior and the possibility to build a six-state memory element, or at least with three readable states, as 180° domains may be hard to distinguish¹². Moreover, the associated long coherence times and localization of magnetic moments are advantages for quantum computing. Indeed the manipulation of the antiferromagnetic order parameter by an ultrafast magneto-optical process with direct coupling opens a route to de-

fine a qbit^{13,14}. The present work aims at harvesting these properties by investigating theoretically the magnetic control of the 'real' compound using spin orbit torques.

The dynamics of antiferromagnets falls in the THz range because the typical resonance frequency can often be approximated by $\sqrt{2\omega_E\omega_a}$ when $\omega_a \ll \omega_E$, where ω_E (resp. ω_a) is the exchange (resp. anisotropy) frequency, defined from its corresponding energy divided by the reduced plank constant \hbar ^{10,15}. For instance, the uniform AF mode around an anisotropy easy axis is known to have an eigenfrequency of $\sqrt{\omega_a(\omega_a + 2\omega_E)}$ ¹⁵ and the mode around the average magnetization \mathbf{m} along the hard axis in the presence of an easy axis has a reported resonance of $\sqrt{2\omega_a\omega_E - \alpha^2\omega_E^2}$, where α is the damping constant¹⁰. Consequently, the AF frequency is at least two orders of magnitude faster than that for ferromagnets. Therefore, interesting applications can be envisioned from this dynamical behavior, including building magnetic oscillators in the THz range and fast-switching memories^{10,15}. Such devices would be insensitive to external magnetic fields and compatible with today's oxide technologies in spintronics. Because NiO is an ideal charge transfer insulator, Joule heating in the writing process can also be minimized. From an experimental perspective, a spin current can be injected by several mechanisms. The most popular uses the spin Hall effect from an adjacent heavy metal, like a Pt stripe, in which an electric current pulse is applied. The generated transverse spin current induces a non-equilibrium spin accumulation at the NiO/Pt interface. The other possibility is dynamical and it relies on the ultra-fast demagnetization of a ferromagnetic layer (FM) by a sufficiently intense femtosecond laser pulse. This generates the fastest and strongest spin pulses available so far^{16,17}, with the extra functionality of setting with the FM magnetization the spin direction in three dimensions. Several parameters have to be adjusted in order to optimize the switching of the NiO layer. It is important to identify the most relevant, resulting in both the lowest STT amplitude and the fastest AF switch. The following section presents a thorough description of the switching processes in a memory element

made of NiO where the full expression of its magnetic anisotropy is considered.

II. NIO CRYSTAL STRUCTURE AND MAGNETIC ANISOTROPY

At room temperature, NiO adopts a fcc structure with Ni^{2+} and O^{2-} at the octahedral sites, altered by a slight rhombohedral contraction along one of the $[111]$ directions. This leads to the formation of four possible twin domains (T-domains)¹⁸. In a given T-domain, the nickel ions spins are subject to various superexchange interactions related to the arrangement of the oxygen ions separating them. They consist in a strong antiferromagnetic coupling at 180° with the six second nearest neighbor (nnn) atoms, as well as a weak ferromagnetic coupling at 90° with the twelve nearest neighbors (nn) atoms, resulting overall in G-type antiferromagnetism with a staggered order along the $[111]$ direction, along which ferromagnetic sheets are stacked¹⁸. The associated energies are $J_{nnn} = -19.01\text{meV}$ for the 6 (spin parallel) next nearest neighbors, $J_{nn}^- = 1.38\text{meV}$ for the 6 (spin parallel) in- (111) -plane nearest neighbors, and $J_{nn}^+ = 1.35\text{meV}$ for the 6 (spin antiparallel) out-of- (111) -plane nearest neighbors¹⁸. The 180° nnn-superexchange being by far the strongest, we neglect here the influence of the nearest neighbor interactions, which is equivalent to looking only at one of the four equivalent sublattices shown in Fig. 1. Even if the nearest neighbor coupling interaction may enrich the magnetization dynamics, it is not treated in the frame of the present paper. Instead, we simply consider that all four sublattices behave similarly.

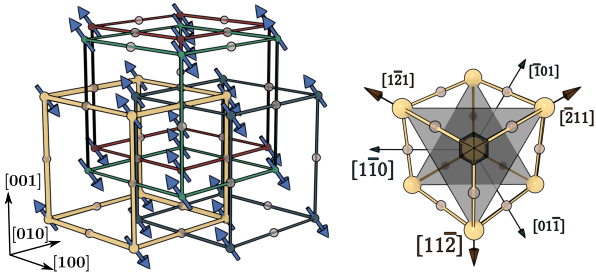


Figure 1. (color online) Crystallographic structure of NiO. On the left: NiO has four distinct 180° superexchange-coupled sublattices (via second nearest neighbors). On the right: NiO main crystallographic axes in the (111) plane.

Within one T-domain, NiO exhibits a rather complex anisotropy pattern with a hard axis along $[111]$, and three easy axes in the $[\bar{2}11]$, $[1\bar{2}1]$ and $[11\bar{2}]$ directions (right panel of Fig. 1), defining three possible S-domains, and 6 possible spin orientations. This configuration is modeled by defining a hard axis \mathbf{u} on top of a cubic anisotropy, thus reflecting the pseudo-cubic symmetry of the crystal, shortened in the $[111]$ diagonal¹⁹. Using subscripts X, Y, Z to denote the projections along the crystallo-

graphic axes $[100]$, $[010]$ and $[001]$ respectively, the effective anisotropy energy for a given spin \mathbf{s} is given by:

$$E_K = K_{1u} (\mathbf{s} \cdot \mathbf{u})^2 + 2K_c (s_X^2 s_Y^2 + s_Y^2 s_Z^2 + s_Z^2 s_X^2) \quad (1)$$

In order to closely fit to the known experimental observations^{10,15,16,19}, we adjust $K_{1u} = 0.08\text{meV}$ and $K_c = 0.02\text{meV}$ in our simulations, so that the return to equilibrium of the Néel vector $\mathbf{l} \equiv \frac{1}{2}(\mathbf{s}_1 - \mathbf{s}_2)$ from a tiny tilt away from rest position, leads to damped oscillations with two characteristic frequencies of 1THz and 0.2THz for a low damping parameter $\alpha = 2.1 \times 10^{-4}$, as shown in Fig. 2. Once projected on the $[111]$ and $[11\bar{2}]$ axes, the equivalent values of the anisotropy energies are 0.0933meV and 0.01meV respectively, which is consistent with the values found in inelastic neutron scattering experiments (0.0972meV and -0.005meV respectively)¹⁸.

It is worth noting from eq. (1), that the equilibrium positions are close to, but not strictly along, the $\langle 11\bar{2} \rangle$ directions to a small out-of-plane deviation (of 3.6° in our case) scaling with the ratio K_c/K_{1u} . This is hard to observe experimentally, and has a negligible influence on the global picture of the magnetic anisotropy of NiO²⁰. Based on this description, we will show that magnetic S-domains can be dynamically switched under realistic spin current pulses.

III. DYNAMIC MODEL

The spin dynamics of antiferromagnets can be described approximately by a set of two coupled Landau Lifshitz Gilbert (LLG) precession equations linking two sublattices of equivalent magnetization²¹. In the case of NiO, it has been predicted theoretically that a spin current should produce a spin transfer torque (STT) acting similarly on the two sublattices and resulting in a significant torque on the Néel vector \mathbf{l} ^{15,21,22}. In order to tackle the dynamics of this antiferromagnetic order, we consider two coupled atomistic equations of motion, one for each equivalent magnetic sublattice labelled by $\hat{\mathbf{s}}$, an unitary vector, that can be formulated as follows²³:

$$\frac{d\hat{\mathbf{s}}}{dt} = \boldsymbol{\omega}_{\text{eff}} \times \hat{\mathbf{s}} \quad (2)$$

By denoting μ_0 the vacuum permeability and γ the gyromagnetic ratio, the effective magnetic field on each sublattice is a functional of $\hat{\mathbf{s}}$, where $\mathbf{H}_{\text{eff}}[\hat{\mathbf{s}}] = \boldsymbol{\omega}_{\text{eff}}[\hat{\mathbf{s}}]/(\mu_0\gamma)$ is composed of the sum of the anisotropy field $\boldsymbol{\omega}_K/(\mu_0\gamma)$, the exchange field $\boldsymbol{\omega}_E/(\mu_0\gamma)$ and the spin torque, altered by the Gilbert damping α :

$$\boldsymbol{\omega}_\Sigma = \boldsymbol{\omega}_K + \boldsymbol{\omega}_E + \hat{\mathbf{s}} \times \boldsymbol{\omega}_\tau \quad (3)$$

$$\boldsymbol{\omega}_{\text{eff}} = \frac{1}{1 + \alpha^2} (\boldsymbol{\omega}_\Sigma - \alpha \boldsymbol{\omega}_\Sigma \times \hat{\mathbf{s}}) \quad (4)$$

In detail, each contribution decomposes as follows:

a. Anisotropy field: Uniaxial and cubic anisotropies are contained in ω_K and by following eq.(1), in the XYZ frame, we find:

$$\omega_K = -\frac{K_{1u}}{\hbar} (\hat{s} \cdot \mathbf{u}) \mathbf{u} - \frac{K_c}{\hbar} \begin{pmatrix} s_X(s_Y^2 + s_Z^2) \\ s_Y(s_X^2 + s_Z^2) \\ s_Z(s_X^2 + s_Y^2) \end{pmatrix} \quad (5)$$

b. Exchange field: The exchange field $\omega_E/(\mu_0\gamma)$ is computed using the Heisenberg model on the first six neighbors of the superexchange lattice (nnn), with $J_{\text{nnn}} = -19.01\text{meV}$ ^{10,18}:

$$\omega_E = \frac{J_{\text{nnn}}}{\hbar} \sum_{j=1}^6 \hat{s}_j \quad (6)$$

c. Spin torque: ω_τ represents the frequency in the Slonczewski's spin transfer torque expression^{21,24}. For spin current \mathbf{j}_s , expressed in $\text{electrons} \cdot \text{m}^{-2} \cdot \text{s}^{-1}$ injected though a thin layer of NiO from an adjacent ferromagnetic layer, we can estimate it as:

$$\omega_\tau \simeq \frac{G}{d} \frac{a^3}{n_s} \mathbf{j}_s \quad (7)$$

where G is the spin transparency at the interface, a the lattice constant, n_s the number of magnetic atoms per unit cell, d the thickness of the layer, and \mathbf{j}_s the spin current. In the present paper, values are expressed directly in spin currents, and the values used for the conversion are $a = 4.177\text{\AA}$, $n_s = 4$, $d = 5\text{nm}$ and $G = 0.1\text{electrons}^{-1}$.

The spin dynamics depends on the relative magnitude and direction of these fields and different behaviors have been reported. The dynamics of a two spins system, antiferromagnetically coupled with a single easy axis and a STT, has been described already in the literature^{10,15}. When the STT is applied perpendicularly to this easy axis, the dynamics produced by eq.(2) is analogous to the dynamics of a damped pendulum subject to gravity (resp. anisotropy) and a driving force (resp. a STT). For a small continuous excitation, the spins stabilize away from the easy anisotropy axis by an angle increasing with the magnitude of the STT. When it overcomes a certain threshold, the AF spins can auto-oscillate around the STT direction^{10,15}. The situation is quite different when the STT is applied along the easy axis. In that case, the AF spins remain aligned along it, until a certain threshold is reached. When the damping force balances the driving force, a small auto-oscillation around the easy axis is obtained, corresponding to the excitation of Kittel modes¹⁵. In this situation, the two sublattices precess with a slightly different angle as the pumped angular momentum unbalances the magnetization of the system. This corresponds to generating circularly polarized magnons with a specific orientation. As reported previously, auto-oscillations can be stabilized by a feedback mechanism happening at the interface with a heavy

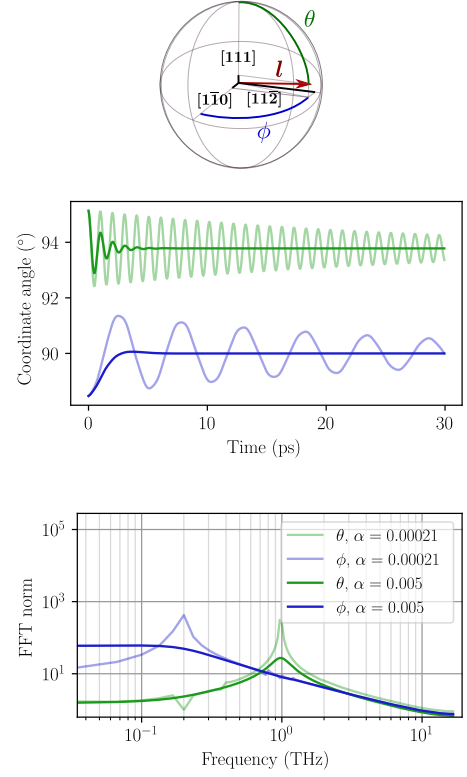


Figure 2. (color online) Spherical coordinates decomposition of the Néel vector (upper panel). Angular dynamics $\theta(t)$ and $\phi(t)$, of the Néel vector of the NiO antiferromagnetic relaxation, starting from a tiny tilt away from equilibrium (middle panel). Fourier transform of the angular dynamics, revealing resonances at 1THz and 0.2THz at low damping $\alpha = 2.1 \times 10^{-4}$. For practical spintronic devices, $\alpha \approx 5 \times 10^{-3}$ is expected and also computed, causing the resonance peaks to flatten and shift (lower panel).

metal²⁵. For an even stronger STT value, the AF vector flips into the perpendicular plane and auto-oscillates around the uncompensated magnetization. This situation is very similar to the spin-flop state under high magnetic fields, with a precession around the field direction.

IV. RESULTS AND DISCUSSION

Within this dynamic model for NiO, a STT applied along the $[111]$ axis of a T-domain can trigger a change of orientation of the spins, switching from one S-domain to another. This is the case studied analytically by Cheng et al.¹⁰ albeit in a simple uniaxial model for the in-plane anisotropy. Our anisotropy profile exhibits 6 possible stable $\langle 11\bar{2} \rangle$ orientations, and a switch at 60° or 180° from one to another can be achieved in picoseconds, as shown in Fig. 3.

Due to the presence of intermediate stable positions, the minimal duration of STT needed to achieve a 180° switch is significantly reduced compared the one pre-

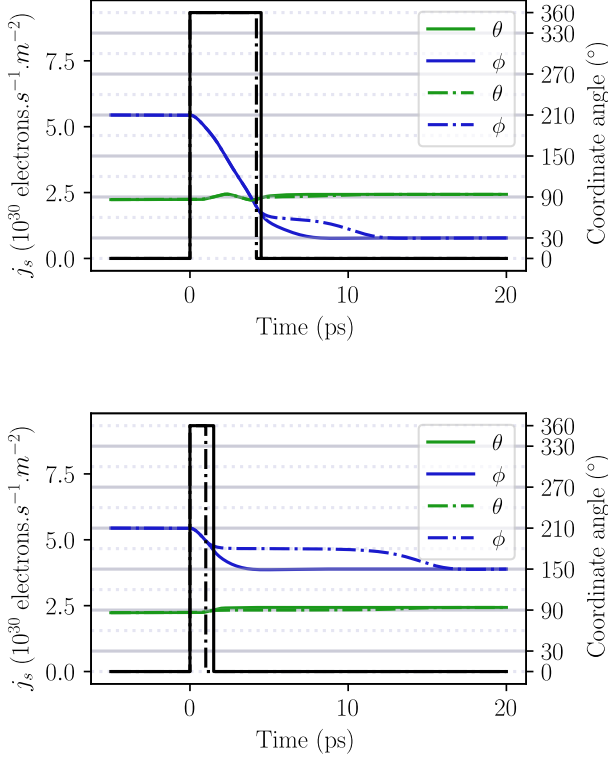


Figure 3. (color online) NiO switching with a STT along [111] of $9.3 \times 10^{30} \text{ electrons.m}^{-2}.\text{s}^{-1}$. Black curves show the switching on and off of the STT. A duration of 4.5ps gives a 180° switch (upper panel), whereas a 1.5ps pulse is enough to trigger a 60° switch (lower panel). The same final θ states can be reached when the pulse durations are reduced to 4.2ps and 1ps respectively, at a cost of a longer relaxation time.

dicted in ref.¹⁰, for the same intensity (3.4GHz). The minimal duration is reevaluated from 10ps to 4.5ps . Even shorter switches can be achieved when considering reorienting the spins by 60° . In this case, the duration of the STT pulse can be reduced to 1ps , for the given intensity.

As the threshold for switching is directly linked to the anisotropy value, the lowest STT amplitude is obtained when the NiO spin trajectories remain in the easy plane. This is achieved when the spin current is polarized along the [111] direction. Cheng et al.¹⁰ obtained an STT threshold close to 3.4GHz ($9.3 \times 10^{30} \text{ electrons.m}^{-2}.\text{s}^{-1}$) whereas it falls down to a smaller value of 1GHz ($1.95 \times 10^{30} \text{ electrons.m}^{-2}.\text{s}^{-1}$) with the more realistic anisotropy model we consider, as shown in Fig. 4.

As long as the STT value stays above the threshold, precession occurs. The higher the STT value, the faster the precession. The precession dynamics depends on how much the system has been driven by the spin torque above the threshold, as well as its natural timescale and damping values. At zero damping, the system oscillates permanently whereas at large damping, it leads to a fast

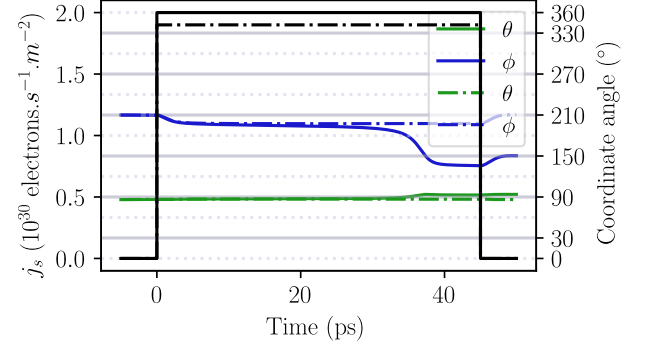


Figure 4. (color online) An STT of $1.9 \times 10^{30} \text{ electrons.m}^{-2}.\text{s}^{-1}$ is below the threshold value to initiate a switch (dotted lines), whereas $2.0 \times 10^{30} \text{ electrons.m}^{-2}.\text{s}^{-1}$ is above the threshold (full lines).

return to the closest equilibrium position, once the spin pumping is turned off. For a more realistic value of $\alpha \approx 0.005$ and by providing a suitable spin pulse strength and duration, all the in-plane equilibrium angles can be reached.

Interestingly, some simple expectations can be inferred directly from the differential equations of motion of the angular dependence of the Néel vector, as shown in appendix B. Firstly, as far as writing speed is targeted, one may realize that for STT pulses sufficiently fast not to lose too much angular momentum in damping processes, i.e. much faster than $1/(2\alpha\omega_E)$, only the total number of injected spins matters. Indeed, the STT contribution cants the two sublattices much faster than the period of a precession. A stable average canting is reached with an exponential decay given by the characteristic time value of $1/(2\alpha\omega_E) = 0.6\text{ps}$, as shown in Fig. 5. A quantity of exchange energy proportional to the number of injected spins at short times is then stored in the system.

Once the excitation is ended and if the accumulated inertia is large enough to overcome the anisotropy energy barrier, the AF vector will explore other equilibrium positions, at a natural precession frequency $\sim \sqrt{2\omega_a\omega_E - \alpha^2\omega_E^2}$.

Fig. 6 shows that the requirement to reach a given memory state depends only on the total number of injected spins, for j_s far from $33 \times 10^{30} \text{ electrons.m}^{-2}.\text{s}^{-1}$ and above the $1.96 \times 10^{30} \text{ electrons.m}^{-2}.\text{s}^{-1}$ threshold (for a 5nm thick NiO). One can conclude that for pulses faster than a few picoseconds, no pulse shaping is necessary and the only parameter governing the switching is just the number of total injected spins. Therefore, the injection can be achieved in an arbitrarily fast time: the shorter the pulse duration is, the stronger the STT strength must be, as shown in Fig. 7. After the injection, the dynamics proceeds, until all the accumulated STT energy stored in the canting is damped, on a timescale determined by α . Consequently, a bit of information can take no more

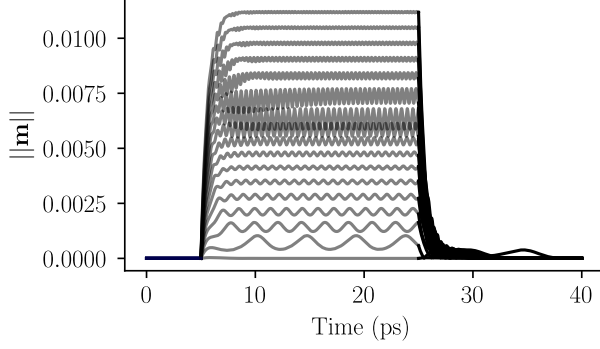


Figure 5. (color online) Evolution of the norm of the average magnetization \mathbf{m} for seventeen different pulses, each 20ps-long with a varying j_s s from 0.3×10^{30} to $53 \times 10^{30} \text{ electrons.m}^{-2}.\text{s}^{-1}$, exhibiting a resonant 2THz oscillation for $j_s = 33 \times 10^{30} \text{ electrons.m}^{-2}.\text{s}^{-1}$, current for which L_θ resonates at 1THz. All the raise and decay stages match an exponential decay law with an identical time constant of 0.6ps.

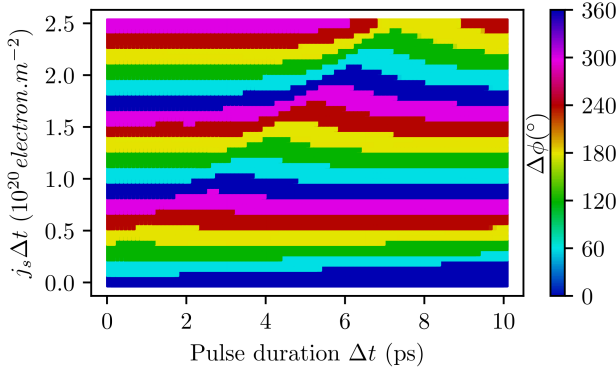


Figure 6. (color online) Final orientation $\Delta\phi$ with respect to the number of injected spins $j_s \Delta t$ and the duration Δt of the injection. Far from $j_s = 33 \times 10^{30} \text{ electrons.m}^{-2}.\text{s}^{-1}$ and above the $1.96 \times 10^{30} \text{ electrons.m}^{-2}.\text{s}^{-1}$ threshold, a constant number of injected spin gives approximately a constant switch.

than a fraction of $2\pi (2\omega_a\omega_E - \alpha^2\omega_E^2)^{-1/2}$ picoseconds to reach a new value, depending on how far from equilibrium the STT ends. Nonetheless, the final rest time to reach a stable state is incompressible and depends on the damping value. As far as stabilization speed is concerned, a too low damping is therefore not desirable, and a value around 0.008 should be optimal¹⁰.

One could thus envision to write a logical bit very fast but a few picosecond waiting time must be observed before re-writing the same bit. As the total rest time is given by the damping term, it is not possible to minimize the total switching procedure duration, for example by changing the direction of the STT to force the AF vector to take a trajectory through higher anisotropy energies.

Moreover, as shown in Fig. 7, for STT directions other than [111], the threshold value is much higher, and while one may be able to reach the new bit position faster, the ringing would last a few picoseconds anyway.

On the other hand, a bipolar pulse would be able to reduce quickly to zero the inertia stored in the canting of the spins, and force the system to reach the equilibrium in a significantly reduced time. This fine tuning, however, seems out of reach experimentally.

Beyond the present simulations, it is important to assess whether or not the conditions for writing such a memory could be achieved experimentally. The shortest spin transfer torque stimulus experimentally available is that generated by the ultra-fast demagnetization of a ferromagnetic layer by a femtosecond laser pulse¹⁷. Emitted from the ferromagnetic layers, bursts of spins have been injected into different metals in double layers (e.g. Fe/Ru or Fe/Au), where their spin conversion generates a THz pulse of electric charge.

In order to estimate what is experimentally achievable, we run simulations using two spin current shapes in the double layers reported in reference¹⁷. The results, displayed in Fig. 8, indicate that the unipolar spin burst in a Fe/Ru structure applied in the [111] direction of NiO, can switch the Néel vector \mathbf{l} to another stable position effectively, whereas the bipolar pulse of the Fe/Au structure cannot.

This is consistent with our previous observation that for such short pulses, only the total amount of injected spins is relevant. For the bipolar pulse, this quantity is too small. Obviously, a real spin current shape cannot be directly deduced from those observed in metallic double layers and a more realistic CoFeB/NiO system should be tested. Indeed, the spin interface transparency with an insulator is reduced compared to that of a pure metal, thus reducing the spin injection efficiency. Nevertheless, as the minimum number of injected spins for switching is four times below that of the experimental spin bursts in Fe/Ru, our simulations indicate that very fast switching should still be possible in NiO, when an adjacent ferromagnetic layer is subjected to ultra-fast demagnetization.

Another interesting dynamical effect can be seen in Fig. 6 where a bump, underlining a reduced efficiency for reaching a final state, appears along a straight line crossing the origin. This thus happens at a fixed spin current, i.e. a fixed precession speed. The explanation to this phenomenon can be found in Figures 5 and 9. It can be seen that the wiggling of the in-plane anisotropy profile, transfers energy into out-of-plane excitations. When this excitation is resonant with the natural out-of-plane precession, around 1THz, the out-of-plane spin excursion gets enhanced and some energy is dissipated in the process. As a consequence, switching is less efficient for this value of spin current and these specific conditions should be avoided for an optimal writing. It is worth noting that our simulations were carried out on an ensemble of two spins only, with periodic boundary conditions in all six directions. In actual experiments, this mechanism should

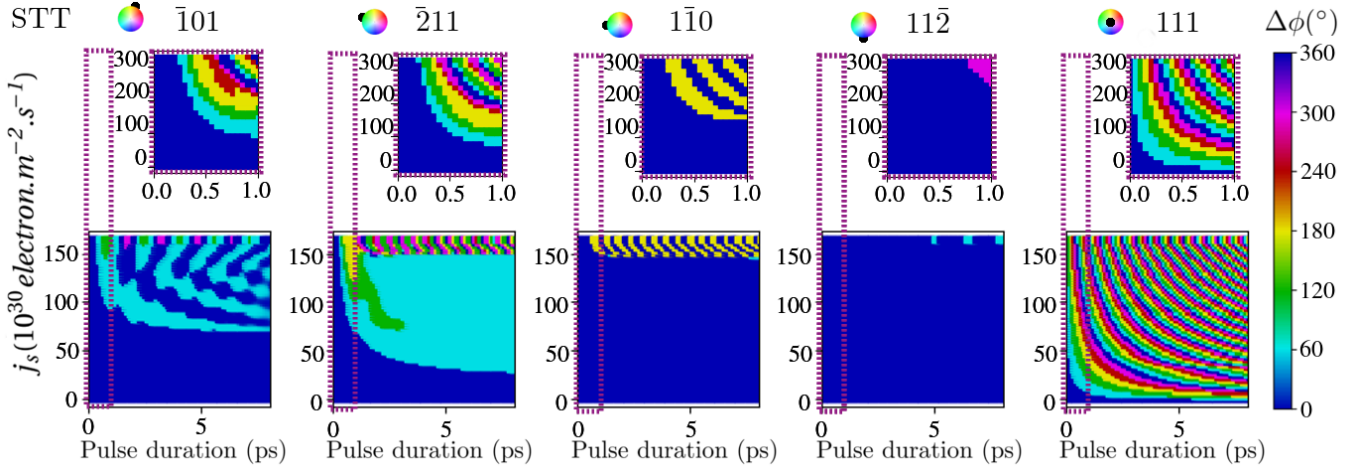


Figure 7. (color online) Domain switch phase diagram for sub-picosecond gate pulses in the main in-plane angles.

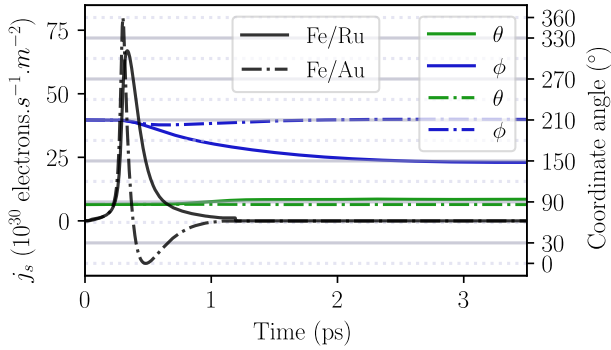


Figure 8. (color online) AF domain switching mechanism after excitation profiles inspired from those computed in Fe/Ru and Fe/Au by reference¹⁷ (see text).

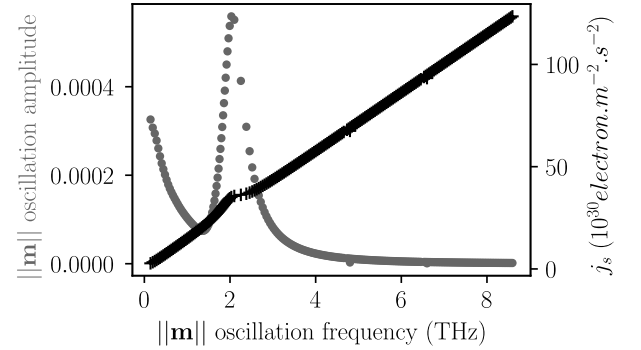


Figure 9. (color online) Amplitude and frequency of the oscillations of $\|\mathbf{m}\|$ for different spin currents.

probably generate out-of-plane magnons.

Finally, long pulses as represented in Fig. 5 can also be applied to THz oscillations as reported in reference¹⁵. For oscillators, the characteristic setting time $1/(2\alpha\omega_E) = 0.6\text{ps}$ must be taken into account before observing stable oscillations. The oscillation frequency varies linearly with the spin current intensity and can be hypothetically adjusted as such. The amplitude of the oscillations is maximal at resonance, for the spin current $j_s = 33 \times 10^{30} \text{ electrons.m}^{-2}\text{s}^{-1}$. The out-of-plane mode at 1THz is excited by the out-of plane excursion of \mathbf{l} during its in-plane rotation, which naturally happens because the trajectory of \mathbf{l} tries to minimize the anisotropy energy along the rhombohedral magnetic anisotropy profile. In steady state rotation, the anisotropy energy is $2\pi/3$ periodic along the trajectory of \mathbf{l} . In the mean time, $\|\mathbf{m}\|$, which varies like $\frac{d\phi}{dt}$ spikes every time \mathbf{l} passes a maximum of energy, namely after every $\pm\langle 1\bar{1}0 \rangle$ directions, and therefore is $2\pi/6$ periodic. As a conse-

quence, at the 1THz resonance of θ , the frequency of $\|\mathbf{m}\|$ is 2THz, and its amplitude is maximal too because $\frac{d\phi}{dt}$ is maximized, as depicted in Fig. 10. This effect is thus purely related to the rhombohedral symmetry of the anisotropy profile we consider. Additionally, Fig. 10 illustrates that for a current just above the threshold, $\|\mathbf{m}\|$ also spikes periodically with high amplitude. For these values, ϕ indeed undergoes rapid changes, but at a lower pace. Hence, the duty cycle is reduced and the harmonicity is degraded.

CONCLUSION

By using atomistic spin simulations, we have shown that a thin layer of NiO can in principle be used to build a 6 state memory device (only three of them may be easily distinguishable). By using magnetic anisotropy expressions that reflect the real symmetry of the material, we have shown that experimentally available sub-

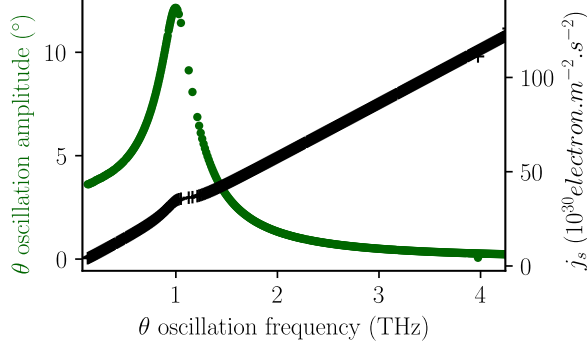


Figure 10. (color online) Amplitude and frequency of the out-of-plane oscillations for different spin currents.

picosecond pulses are *a priori* adequate to switch a 5nm thick memory element. We propose a device formed by a NiO/ferromagnetic double layer, where an ultrafast laser is used to inject a spin population at an arbitrary spin angle, by demagnetizing the ferromagnetic layer. Both constraints on the growth of epitaxial NiO, as well as the easy control of the STT direction are then released. This excitation process shows the possibility to access deterministically the six AF spin states, allowed by the magnetic anisotropy of NiO at picoseconds speed. Beyond memory devices, the non-trivial magnetic anisotropy of NiO suggests a richer dynamics that could lead to other spintronic applications in the THz range.

ACKNOWLEDGMENTS

We wish to acknowledge Julien Tranchida for the fruitful discussions, and the French National Research Agency for support with the project via SANTA (Grant No.ANR-18-CE24-0018-03).

Appendix A: Numerical implementation

Simulations are performed for two spins that are coupled with effective fields. Each spin represents its own ferromagnetic sublattice. The equations of precession are integrated in time with a symplectic integrator. The transverse equation (2) is discretized to update only the orientation of each spin for a given timestep Δt . In practice, $\mathbf{s}_{t+\Delta t}$ is computed from \mathbf{s}_t and $\boldsymbol{\omega}_{\text{eff}}$ with $\mathcal{O}(\Delta t^3)$ precision²³, according to:

$$\mathbf{s}_{t+\Delta t} = \frac{1}{1 + \frac{1}{4}(\Delta t)^2 \boldsymbol{\omega}_{\text{eff}}^2} \left[\mathbf{s}_t + \Delta t (\boldsymbol{\omega}_{\text{eff}} \times \mathbf{s}_t) + \frac{1}{4} (\Delta t)^2 (2 (\boldsymbol{\omega}_{\text{eff}} \cdot \mathbf{s}_t) \boldsymbol{\omega}_{\text{eff}} - \boldsymbol{\omega}_{\text{eff}}^2 \mathbf{s}_t) \right] \quad (\text{A1})$$

To check the consistence of this approach, we evaluate the dynamics of the Néel vector and average magnetization by using the numerical values found in reference^{10,25}. Our simulations reproduce well the published results as shown in Fig. 11.

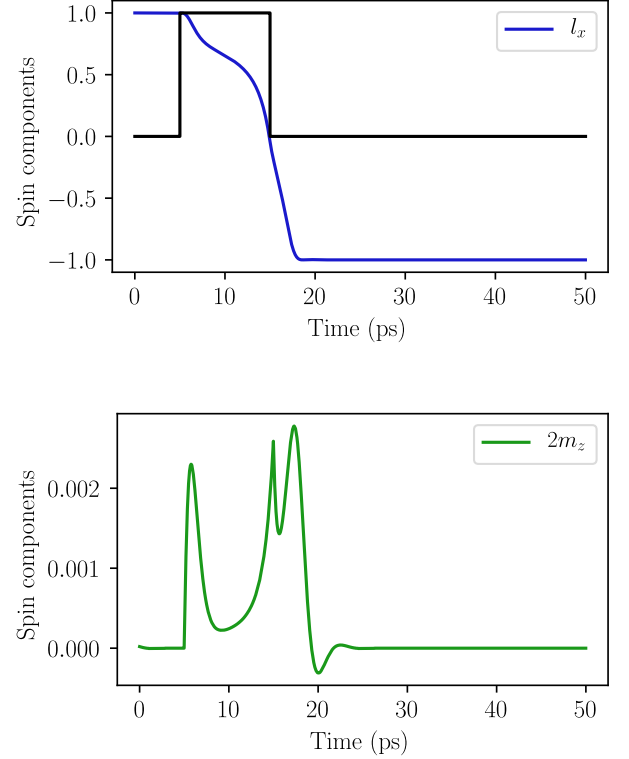


Figure 11. (color online) Reproduction of the switching process described in reference¹⁰. The upper panel displays the STT pulse (in black), the x-component of the Néel vector \mathbf{l} (in blue). The lower panel displays the z-component of twice the average AF magnetization \mathbf{m} .

Appendix B: Raising time in an uniaxial anisotropy

By considering a unique easy axis (ω_a along x) in a hard plane (ω_A along z), as long as $|\mathbf{m}| \ll |\mathbf{l}|$, the equation for \mathbf{l} reduces to a one dimensional problem¹⁰:

$$\frac{d^2\phi}{dt^2} + 2\alpha\omega_E \frac{d\phi}{dt} + \frac{\omega_R^2}{2} \sin(2\phi) = 2\omega_E\omega_\tau, \quad (\text{B1})$$

with $\omega_R \equiv \sqrt{2\omega_a\omega_E}$. The out-of-plane component of the magnetization vector is simply $m_z = -(2\omega_E + |\omega_A| + \omega_a l_x^2)^{-1} \frac{d\phi}{dt}$. With $\phi(0) = 0$ and by considering the response near the beginning of the pulse, for which $\phi \ll 2\pi$, the previous differential equation is linearized, such as:

$$\frac{d^2\phi}{dt^2} + 2\alpha\omega_E \frac{d\phi}{dt} + \omega_R^2 \phi = 2\omega_E\omega_\tau, \quad (\text{B2})$$

and solved, after defining $\omega_{ip} = \sqrt{2\omega_a\omega_E - \alpha^2\omega_E^2}$. We find

$$\phi(t) = \frac{\omega_\tau}{\omega_a} \left(1 - e^{-\alpha\omega_E t} \left[\cos(\omega_{ip}t) + \frac{\alpha\omega_E}{\omega_{ip}} \sin(\omega_{ip}t) \right] \right) \quad (\text{B3})$$

Therefore near $t = 0$,

$$\frac{d\phi}{dt} \sim 2\omega_\tau\omega_E t, \quad (\text{B4})$$

meaning that from reference¹⁵, a simple model for the convergence to the average value of the angular velocity $\frac{\omega_\tau}{\alpha} (1 - e^{-t/\tau_c})$ gives $\tau_c = 1/(2\alpha\omega_E) \sim 0.6\text{ps}$, which is in agreement with our numerical simulations, as depicted in Fig. 5 in section IV.

-
- * theophile.chirac@umontpellier.fr; Now at Laboratoire Charles Coulomb, UMR 5221 CNRS-Université de Montpellier, F-34095 Montpellier, France
- † jean-yves.chauleau@cea.fr
- ‡ pascal.thibaudeau@cea.fr
- § michel.viret@cea.fr
- ¹ T. Jungwirth, X. Marti, P. Wadley, and J. Wunderlich, *Nature Nanotechnology* **11**, 231 (2016).
 - ² A. S. Núñez, R. A. Duine, P. Haney, and A. H. MacDonald, *Phys. Rev. B* **73**, 214426 (2006).
 - ³ P. M. Haney, D. Waldron, R. A. Duine, A. S. Núñez, H. Guo, and A. H. MacDonald, *Phys. Rev. B* **75**, 174428 (2007).
 - ⁴ R. A. Duine, P. M. Haney, A. S. Núñez, and A. H. MacDonald, *Phys. Rev. B* **75**, 014433 (2007).
 - ⁵ C. Marrows, *Science* **351**, 558 (2016).
 - ⁶ P. Wadley, B. Howells, J. Železný, C. Andrews, V. Hills, R. P. Campion, V. Novák, K. Olejník, F. Maccheronzi, S. S. Dhesi, S. Y. Martin, T. Wagner, J. Wunderlich, F. Freimuth, Y. Mokrousov, J. Kuneš, J. S. Chauhan, M. J. Grzybowski, A. W. Rushforth, K. W. Edmonds, B. L. Gallagher, and T. Jungwirth, *Science* **351**, 587 (2016).
 - ⁷ C. Hahn, G. de Loubens, V. V. Naletov, J. B. Youssef, O. Klein, and M. Viret, *EPL (Europhysics Letters)* **108**, 57005 (2014).
 - ⁸ H. Wang, C. Du, P. C. Hammel, and F. Yang, *Phys. Rev. B* **91**, 220410 (2015).
 - ⁹ R. Lebrun, A. Ross, S. A. Bender, A. Qaiumzadeh, L. Baldatti, J. Cramer, A. Brataas, R. A. Duine, and M. Kläui, *Nature* **561**, 222 (2018).
 - ¹⁰ R. Cheng, M. W. Daniels, J.-G. Zhu, and D. Xiao, *Phys. Rev. B* **91**, 064423 (2015).
 - ¹¹ E. Uchida, N. Fukuoka, H. Kondoh, T. Takeda, Y. Nakazumi, and T. Nagamiya, *Journal of the Physical Society of Japan* **23**, 1197 (1967).
 - ¹² V. Baltz, A. Manchon, M. Tsoi, T. Moriyama, T. Ono, and Y. Tserkovnyak, *Rev. Mod. Phys.* **90**, 015005 (2018).
 - ¹³ N. P. Duong, T. Satoh, and M. Fiebig, *Phys. Rev. Lett.* **93**, 117402 (2004).
 - ¹⁴ F. Meier, J. Levy, and D. Loss, *Physical Review B* **68**, 134417 (2003).
 - ¹⁵ F. Keffer and C. Kittel, *Phys. Rev.* **85**, 329 (1952); A. J. Sievers and M. Tinkham, *Phys. Rev.* **129**, 1566 (1963);

- R. Khymyn, I. Lisenkov, V. Tiberkevich, B. A. Ivanov, and A. Slavin, *Scientific Reports* **7**, 43705 (2017).
- ¹⁶ T. Kampfrath, A. Sell, G. Klatt, A. Pashkin, S. Mährlein, T. Dekorsy, M. Wolf, M. Fiebig, A. Leitenstorfer, and R. Huber, *Nature Photonics* **5**, 31 (2010).
- ¹⁷ T. Kampfrath, M. Battiato, P. Maldonado, G. Eilers, J. Nötzold, S. Mährlein, V. Zbarsky, F. Freimuth, Y. Mokrousov, S. Blügel, M. Wolf, I. Radu, P. M. Oppeneer, and M. Münzenberg, *Nature Nanotechnology* **8**, 256 (2013).
- ¹⁸ M. T. Hutchings and E. J. Samuelsen, *Phys. Rev. B* **6**, 3447 (1972).
- ¹⁹ J. Milano, L. B. Steren, and M. Grimsditch, *Phys. Rev. Lett.* **93**, 077601 (2004); T. Satoh, S.-J. Cho, R. Iida, T. Shimura, K. Kuroda, H. Ueda, Y. Ueda, B. A. Ivanov, F. Nori, and M. Fiebig, *Phys. Rev. Lett.* **105**, 077402 (2010); S. Baierl, J. H. Mentink, M. Hohenleutner, L. Braun, T.-M. Do, C. Lange, A. Sell, M. Fiebig, G. Woltersdorf, T. Kampfrath, and R. Huber, *Phys. Rev. Lett.* **117**, 197201 (2016); T. Kohmoto and T. Moriyasu, in *2018 43rd International Conference on Infrared, Millimeter, and Terahertz Waves (IRMMW-THz)* (2018) pp. 1–2.
- ²⁰ T. Yamada, S. Saito, and Y. Shimomura, *Journal of the Physical Society of Japan* **21**, 672 (1966), <https://doi.org/10.1143/JPSJ.21.672>.
- ²¹ S. Chikazumi, *Physics of Ferromagnetism*, International Series of Monographs on Physics (Oxford Science Publications, 1997); H. V. Gomonay and V. M. Loktev, *Phys. Rev. B* **81**, 144427 (2010).
- ²² R. Cheng, J. Xiao, Q. Niu, and A. Brataas, *Phys. Rev. Lett.* **113**, 057601 (2014).
- ²³ J. Tranchida, S. Plimpton, P. Thibaudeau, and A. Thompson, *Journal of Computational Physics* **372**, 406 (2018).
- ²⁴ J. Slonczewski, *Journal of Magnetism and Magnetic Materials* **159**, L1 (1996).
- ²⁵ R. Cheng, D. Xiao, and A. Brataas, *Phys. Rev. Lett.* **116**, 207603 (2016); R. Cheng, J.-G. Zhu, and D. Xiao, *Phys. Rev. Lett.* **117**, 097202 (2016); T. Nussle, P. Thibaudeau, and S. Nicolis, *Phys. Rev. B* **100**, 214428 (2019), [arXiv:1907.01857](https://arxiv.org/abs/1907.01857).